Anal. Chem. **2002,** *74,* 3760−3771

Influence of Charge State on Product Ion Mass Spectra and the Determination of 4S/6S Sulfation Sequence of Chondroitin Sulfate Oligosaccharides

Joseph E. McClellan, Catherine E. Costello, Peter B. O'Connor, and Joseph Zaia*

Mass Spectrometry Resource, Department of Biochemistry, Boston University School of Medicine, 715 Albany St., R-806, Boston, Massachusetts 02118

Electrospray ionization-Fourier transform ion cyclotron resonance tandem mass spectrometry is used to study the influence of charge state on the product ion spectra of chondroitin sulfate oligosaccharides for determination of the sulfate position on *N*-acetylgalactosamine residues. Sustained off-resonance irradiation collision-induced dissociation and infrared multiphoton dissociation are investigated for tandem mass spectrometry of chondroitin sulfate. Product ion spectra were obtained for ions of varying charge states from (4,5)-unsaturated (Δ-unsaturated), reduced Δ-unsaturated, and saturated oligosaccharides from chondroitin sulfate A and chondroitin sulfate C, separately. It was observed that ions in which the charge (*z*) is less than the number of sulfates dissociate to produce predominantly even-numbered B_n, C_n, Y_n, and Z_n ions, and that odd-numbered fragment ions are observed for ions that have *z* equal to the number of sulfates. Sulfate adducted ions were observed in the product ion spectra of singly charged tetramer and hexamer oligosaccharides. This sulfate adduction was determined to result from migration of neutral sulfate during excitation.

Glycosaminoglycans (GAGs) are linear polymers of repeating disaccharide units that are attached to proteoglycan core proteins and may be found prominently on cell surfaces and within the extracellular matrix (ECM) of all tissues in virtually every animal species.[1−7] GAGs play an intricate role in the modulation of cell signals; assist in the regulation of cell growth and differentiation through interactions with cytokines; bind signal transducers; and act as reservoirs, scavengers, or cofactors for cell signaling.[8] Types of sulfated GAGs include chondroitin sulfate, dermatan sulfate, heparan sulfate, and keratan sulfate. The fine structure of GAG chains is quite diverse as the result of maturation reactions involving sulfation, epimerization, and glycosylation, which are dependent on cell type and not the core protein.

A wide variety of proteoglycans contain chondroitin sulfate (CS) linked to serine residues via a xylose-containing linker. CS consists of repeating units of -GlcA(β1,3)GalNAc(β1,4)- polymerized in chains of 20−50 kDa sizes, depending on the core protein and tissue location. Examples of CS-containing proteoglycans include the hyalectins (aggrecan, versican, neurocan, brevican), small leucine-rich proteoglycans (decorin and biglycan), bamacan (a basement membrane proteoglycan), and syndecan (a cell surface proteoglycan also modified with heparin sulfate). CS chains are expressed with 4-sulfated and 6-sulfated domains, the patterns of which are known to be tissue-specific.[9] There is evidence to suggest that CS isoforms differing in the position and degree of sulfation play distinct functional roles during development.[10] Monoclonal antibodies have been used to map functionally distinct tissue domains[11] and demonstrate patterned expression of CS epitopes. In addition, CS epitopes are distributed in a nonrandom manner within CS chains, possibly facilitating interactions with respondent proteins.[12] For cartilage aggrecan, changes in CS chain length and sulfation pattern have been correlated with tissue remodeling during skeletal development,[13,14] aging,[15] and development of osteoarthritis.[16] Changes have been demonstrated to the nonreducing terminal saccharides of CS chains,[17] to the linker region,[18,19] and to the CS core domain.[20]

* Corresponding author. Phone: 617-638-6762. Fax: 617-638-6760. Email: jzaia@bu.edu.

(1) Kraemer, P. M. *Biochemistry* **1971**, *10*, 1445−1451.
(2) Kraemer, P. M. *Biochemistry* **1971**, *10*, 1437−1445.
(3) Nader, H. B.; Ferreira, T. M.; Toma, L.; Chavante, S. F.; Dietrich, C. P.; Casu, B.; Torri, G. *Carbohydr. Res.* **1988**, *184*, 292−300.
(4) Bernfield, M.; Gotte, M.; Park, P. W.; Reizes, O.; Fitzgerald, M. L.; Lincecum, J.; Zako, M. *Annu. Rev. Biochem.* **1999**, *68*, 729−77.
(5) Perrimon, N.; Bernfield, M. *Nature* **2000**, *404*, 725−8.
(6) Iozzo, R. V. *Proteoglycans: structure, biology and molecular interactions*; Marcel Dekker: New York, 2000.
(7) Nugent, M. A. *Proc. Natl. Acad. Sci. U.S.A.* **2000**, *97*, 10301−10303.
(8) Varki, A.; Cummings, R.; Esko, J.; Freeze, H.; Hart, G.; Marth, G. *Essentials of Glycobiology*; Cold Spring Harbor Laboratory Press: Cold Spring Harbor, NY, 1999.
(9) Cheng, F.; Heinegard, D.; Malmstrom, A.; Schmidtchen, A.; Yoshida, K.; Fransson, L. A. *Glycobiology* **1994**, *4*, 685−696.
(10) Mark, M. P.; Butler, W. T.; Ruch, J. V. *Dev. Biol.* **1989**, *133*, 475−488.
(11) Sorrell, J. M.; Mahmoodian, F.; Schafer, I. A.; Davis, B.; Caterson, B. *J. Histochem. Cytochem.* **1990**, *38*, 393−402.
(12) Sorrell, J. M.; Carrino, D. A.; Caplan, A. I. *Matrix* **1993**, *13*, 351−361.
(13) Roughley, P. J.; White, R. J. *J. Biol. Chem.* **1980**, *255*, 217−224.
(14) Thonar, E. J.; Buckwalter, J. A.; Kuettner, K. E. *J. Biol. Chem.* **1986**, *261*, 2467−2474.
(15) Bayliss, M. T.; Osborne, D.; Woodhouse, S.; Davidson, C. *J. Biol. Chem.* **1999**, *274*, 15892−15900.
(16) Shinmei, M.; Miyauchi, S.; Machida, A.; Miyazaki, K. *Arthritis Rheum.* **1992**, *35*, 1304−1308.
(17) Plaas, A. H.; Wong-Palms, S.; Roughley, P. J.; Midura, R. J.; Hascall, V. C. *J. Biol. Chem.* **1997**, *272*, 20603−20610.
(18) Shibata, S.; Midura, R. J.; Hascall, V. C. *J. Biol. Chem.* **1992**, *267*, 6548−6555.
(19) Lauder, R. M.; Huckerby, T. N.; Nieduszynski, I. A. *Biochem. J.* **2000**, *347*, 339−348.

10.1021/ac025506+ CCC: $22.00
Published on Web 06/27/2002

The heterogeneity of GAG structures renders them difficult to purify and hinders attempts to discover both structural determinants for the binding of proteins and the binding affinities for these structures. Currently, there are limited analytical tools and methods for the structural characterization and sequencing of GAGs.[21] The average composition of GAG chains can be determined after chemical or enzymatic digestion of the biopolymer by using paper electrophoresis,[22] high-performance liquid chromatography,[23] or capillary electrophoresis;[24] however, it is not possible to determine directly the composition of the individual oligosaccharides making up the GAG distribution using minimal sample amounts. Direct structural determination of CS oligosaccharides using nuclear magnetic resonance (NMR) spectroscopy has been demonstrated.[25−28] NMR requires milligram quantities of pure oligosaccharide and is not suitable for the analysis of complex mixtures. Matrix-assisted laser desorption/ionization (MALDI) time-of-flight (TOF) mass spectrometry has been used to determine the sequences of purified GAG molecules.[21,29] This technique involves pairing the oligosaccharide with a basic peptide and determining the mass of the peptide−oligosaccharide complex.[30,31] By measuring the mass before and after partial enzymatic or chemical digestion, it is possible to determine the oligosaccharide residue sequence; however, this method is limited by its need for extensive purification prior to analysis. GAGs have been observed to produce abundant negative ions using electrospray ionization (ESI) MS.[32−34]

Mass spectrometric differentiation of positional sulfation isomers has been demonstrated for CS-derived disaccharides containing a (4,5) double bond at the nonreducing terminus, ΔUroA-(β1,3)-D-GalNAc4S (ΔDi4S) and ΔUroA(β1,3)-D-GalNAc6S (ΔDi6S), using negative ion fast atom bombardment (FAB) collision-induced dissociation (CID).[35] This work has been extended to negative ionization electrospray using quadrupole ion trap[36,37] and triple quadrupole[38] instruments to show that the ESI tandem mass spectrometry (MS/MS) can be used to determine sulfation ratios in mixtures produced by chondroitin lyases without derivatization or purification.

Most recently, our laboratory has developed methods using size-exclusion chromatography (SEC) and tandem mass spectrometry for the determination of sulfation position in CS oligosaccharides.[38,39] CS type A (CSA) is sulfated primarily (90%) at the 4 position of GalNAc, and CS type C (CSC) is sulfated primarily (90%) at the 6 position. Oligosaccharides prepared from CSA and CSC produce distinct patterns of product ion abundances in CID-MS/MS spectra that allow the determination of sulfate position for individual GalNAc residues.[39] For ions in which all sulfate groups are deprotonated (z = the number of sulfates), abundant ions corresponding to glycosidic bond cleavages are observed.[39] These glycosidic bond cleavages are observed at low collision energy, under which conditions ions corresponding to sulfate losses are very low in abundance. Glycosidic bond cleavages are observed at the reducing side of the UroA residues but not at the reducing side of the GalNAc residues, resulting in the production of odd-numbered B_n and Y_n ions. Therefore, it is possible to determine the sulfate position at each GalNAc (except for the GalNAc at the nonreducing terminus) of CS oligosaccharides from the product ion spectra of the fully charged ion. This has been demonstrated for CS chains varying in length from tetramers to octamers.

To date, the influences of charge state on the product ion patterns generated from CS oligosaccharides have not been determined. The present work uses ESI-Fourier transform ion cyclotron resonance (FT-ICR) MS and MS/MS to show that the charge state of a given CS oligosaccharide dramatically affects the product ion pattern generated there from. This work takes advantage of ESI source conditions that can be set to favor formation of charge states where not all of the sulfate groups are charged (z < the number of sulfates). Further, the ability to determine the sulfate position at the nonreducing terminus GalNAc is investigated. The long-term aim of this work is to demonstrate that binding interactions between proteins and GAGs can be studied using tandem mass spectrometry. Because this entails analysis of extended sequences (up to 20-mers), a series of increasing oligosaccharide lengths are studied in this paper.

EXPERIMENTAL SECTION

Samples. Oligosaccharides from CS of varying lengths were investigated using negative ion ESI-FT-ICR MS and MS/MS. CSA and CSC (Seikagaku/Associates of Cape Cod, Falmouth, MA) were each digested enzymatically to produce saturated, Δ-unsaturated, and reduced Δ-unsaturated saccharides. These saccharides included the disaccharide, tetrasaccharide, and hexasaccharide. ESI-FT-ICR MS and MS/MS spectra were also acquired from ΔDi4S and ΔDi6S disaccharide standards (Seikagaku/Associates of Cape Cod, Falmouth, MA).

Preparation of Saturated Chondroitin Sulfate Saccharides. CSA and CSC were digested separately with testicular hyaluronidase and fractionated using SEC as previously described.[38] Testicular hyaluronidase cleaves to the reducing side of GalNAc

(20) Plaas, A. H.; West, L. A.; Wong-Palms, S.; Nelson, F. R. *J. Biol. Chem.* **1998**, *273*, 12642−12649.
(21) Venkataraman, G.; Shriver, Z.; Raman, R.; Sasisekharan, R. *Science* **1999**, *286*, 5375−42.
(22) Guo, Y. C.; Conrad, H. E. *Anal. Biochem.* **1989**, *176*, 96−104.
(23) Linhardt, R. J.; Turnbull, J. E.; Wang, H. M.; Loganathan, D.; Gallagher, J. T. *Biochemistry* **1990**, *29*, 2611−2617.
(24) Ampofo, S. A.; Wang, H. M.; Linhardt, R. J. *Anal. Biochem.* **1991**, *199*, 249−255.
(25) Chai, W.; Kogelberg, H.; Lawson, A. M. *Anal. Biochem.* **1996**, *237*, 88−102.
(26) Kinoshita, A.; Yamada, S.; Haslam, S. M.; Morris, H. R.; Dell, A.; Sugahara, K. *J. Biol. Chem.* **1997**, *272*, 19656−19665.
(27) Kitagawa, H.; Tanaka, Y.; Yamada, S.; Seno, N.; Haslam, S. M.; Morris, H. R.; Dell, A.; Sugahara, K. *Biochemistry* **1997**, *36*, 3998−4008.
(28) Chai, W.; Lawson, A. M.; Gradwell, M. J.; Kogelberg, H. *Eur. J. Biochem.* **1998**, *251*, 114−121.
(29) Shriver, Z.; Raman, R.; Venkataraman, G.; Drummond, K.; Turnbull, J.; Toida, T.; Linhardt, R.; Biemann, K.; Sasisekharan, R. *Proc. Natl. Acad. Sci. U.S.A.* **2000**, *97*, 10359−10364.
(30) Juhasz, P.; Biemann, K. *Proc. Natl. Acad. Sci. U.S.A.* **1994**, *91*, 4333−4337.
(31) Juhasz, P.; Biemann, K. *Carbohydr. Res.* **1995**, *270*, 131−147.
(32) Takagaki, K.; Kojima, K.; Majima, M.; Nakamura, T.; Kato, I.; Endo, M. *Glycoconjugate J.* **1992**, *9*, 174−179.
(33) Chai, W.; Luo, J.; Lim, C. K.; Lawson, A. M. *Anal. Chem.* **1998**, *70*, 2060−2066.
(34) Kim, Y. S.; Ahn, M. Y.; Wu, S. J.; Kim, D. H.; Toida, T.; Teesch, L. M.; Park, Y.; Yu, G.; Lin, J.; Linhardt, R. J. *Glycobiology* **1998**, *8*, 869−877.
(35) Lamb, D. J.; Wang, H. M.; Mallis, L. M.; Linhardt, R. J. *J. Am. Soc. Mass Spectrom.* **1992**, *3*, 797−803.
(36) Desaire, H.; Leary, J. *J. Am. Soc. Mass Spectrom.* **2000**, *11*, 916−920.
(37) Desaire, H.; Sirich, T. L.; Leary, J. A. *Anal. Chem.* **2001**, *73*, 3513−3520.
(38) Zaia, J.; Costello, C. E. *Anal. Chem.* **2001**, *73*, 233−239.
(39) Zaia, J.; McClellan, J. E.; Costello, C. E. *Anal. Chem.* **2001**, *73*, 6030−6039.

residues by a hydrolytic mechanism and produces saturated oligosaccharides from tetramers to dodecamers. Oligosaccharides produced by enzymatic degradation of CSA and CSC were collected separately into pure fractions containing dimers, tetramers, and hexamers.

Preparation of Δ-Unsaturated Chondroitin Sulfate Saccharides. CSA and CSC were digested separately with chondroitinase ACI (Seikagaku/Associates of Cape Cod, Falmouth, MA) and fractionated using SEC as previously described.[38] Chondroitinase ACI cleaves to the reducing side of GalNAc residues by an eliminative mechanism and produces oligosaccharides with a (4,5) double bond at the nonreducing terminus, known as a Δ-unsaturation. Oligosaccharides produced by enzymatic degradation of CSA and CSC were collected separately into pure fractions containing dimers, tetramers, and hexamers.

Preparation of Reduced Δ-Unsaturated Chondroitin Sulfate Saccharides. CSA and CSC were digested separately with chondroitinase ACI, reduced with sodium borodeuteride (Aldrich Chemical Co., Milwaukee, WI), and then fractionated using SEC as previously described.[39] Oligosaccharides produced by enzymatic degradation of CSA and CSC were collected separately into pure fractions containing dimers, tetramers, and hexamers.

Electrospray Ionization (Nanospray) Mass Spectrometry. All digested fractions were dried on a Savant Instruments SC110 Speedvac concentrator (Holbrook, NY) and then dissolved in a solution of 65:35:0.1 (v/v/v) water/methanol/ammonium hydroxide for mass analysis in negative ion mode by ESI-FT-ICR MS. All experiments were performed on a modified IonSpec HiResESI mass spectrometer (Irvine, CA) equipped with a 7 Tesla active-shielded superconducting electromagnet and a home-built nanospray ion source. Nanospray needles were pulled to 1−2-μm i.d. tips from thin-walled borosilicate glass capillaries (1.2-mm o.d., 0.90-mm i.d.; World Precision Instruments, Sarasota, FL) using a Sutter Instrument P 80/PC micropipet puller (San Rafael, CA). The nanospray needles were positioned at different locations, either closer to or farther from the orifice of the mass spectrometer, to influence the charge state of the CS oligomers. Sample solutions were sprayed by grounding the solution and ramping the orifice potential to 600−800 V positive relative to the solution. The voltage used depended on the location of the nanospray needle to the orifice, with lower voltages used for closer needle positions. The ion source conditions were adjusted to optimize signal intensity, minimize in-source fragmentation, and produce multiple ion charge states for the larger oligosaccharides.

For all ESI-FT-ICR MS and MS^n experiments, the capillary exit potential and the skimmer were set at −75 and −15 V, respectively. The hexapole offset potential was set at −9.25 V, both the hexapole exit potential and the quadrupole offset potential were set at 0.00 V, and the shutter was biased at −75 V. To trap ions in the ICR cell, the quadrupole trapping plate was set at −10 V, and a gas pulse (8 Torr back pressure) was introduced for 4 ms to raise the pressure in the analyzer region to $\sim 1 \times 10^{-6}$ Torr. The excitation event occurred over an m/z range of 80−2000 for 4.0 ms at 110 V_{b-p}. Direct mode detection was used with 4 MHz sampling into 512 K data points. Each presented mass spectrum represents the summing of 5 scans. Although there is variability in S/N among the mass spectra, because of differences in sample concentration and charge state distribution, each acquisition is representative of a reproducible set of experiments.

Tandem Mass Spectrometry. FT-ICR MS offers several possible fragmentation techniques for performing MS/MS and MS^n experiments, including both sustained off-resonance irradiation collision-induced dissociation (SORI-CID)[40] and infrared multiphoton dissociation (IRMPD).[41,42] Product ion mass spectra were obtained for ions corresponding to disaccharides, tetrasaccharides, and hexasaccharides generated from each of the digestion preparations. Notched waveforms from the arbitrary waveform generator were applied to excite and eject all unwanted ions and isolate the frequency range of interest. Generally, one arbitrary waveform was sufficient to isolate cleanly the ion of interest. In cases in which two waveforms were necessary, the first arbitrary waveform was used to perform a coarse isolation, and a second was used to perform a fine isolation.

SORI-CID is a general method of collisionally activating ions for fragmentation by irradiating them with a single off-resonant sine wave excitation waveform while the background gas pressure is raised to $\sim 1 \times 10^{-6}$ Torr.[40] To excite and fragment the ions of interest, a waveform was applied using a frequency offset ($\Delta\nu$) at 1.5% of the reduced cyclotron frequency,[43] which ranged from 3.51 kHz for m/z 458.06 to 1.15 kHz for m/z 1394.21. The collision gas used for CID was N_2, which was pulsed 100 ms prior to the SORI event for 4 ms. The SORI waveform was applied for 1000 ms and had an amplitude ranging from 6 to 9 V_{b-p}. Previous experiments in this laboratory have shown that, 10 V_{b-p} is optimal for the dissociation of carbohydrate, glycolipid, and polypeptide samples over a m/z range of 300−3500 via SORI-CID using a $\Delta\nu$ of 1.5%.[43] A lower amplitude was used in the analysis of CS oligosaccharides because of their fragility and concerns of over fragmentation. For IRMPD, a 75 W CO_2 laser (Synrad, Mukilteo, WA) was used to generate infrared photons, which enter the ICR cell on-axis, and subsequently heat and fragment trapped ions of interest. Irradiation was performed over a time range of 50−500 ms with the laser set at 100% power.

RESULTS AND DISCUSSION

Oligosaccharides produced by enzymatic degradation of CSA and CSC were fractionated using SEC, resulting in pure dimer, tetramer, and hexamer fractions. In theory, Δ-unsaturated CS oligosaccharides (produced by chondroitinases) would yield isobaric C_n and Z_n ions where n is an even number, and saturated CS oligosaccharides (produced by testicular hyaluronidase) would generate isobaric B_n and Z_n ions and isobaric C_n and Y_n ions where n is even. Established nomenclature is used to designate product ions.[44] Reduced Δ-unsaturated CS oligosaccharides, however, should fragment into unique calculated m/z values for B_n, C_n, Y_n, and Z_n ions. (See Table 1.) Saturated CS oligosaccharides differ in structure from the Δ-unsaturated CS oligosaccharides at the nonreducing end and from the reduced Δ-unsaturated CS oli-

(40) Gauthier, J. W.; Trautman, T. R.; Jacobsen, D. B. *Anal. Chim. Acta* **1991**, *246*, 1363−1367.
(41) Basov, N. G.; Markin, E. P.; Oraevski, A. N.; Pantratov, A. V.; Shachkov, A. N. *JETP Lett.* **1971**, *14*, 165−169.
(42) Little, D. P.; Speir, J. P.; Senko, M. W.; O'Connor, P. B.; McLafferty, F. W. *Anal. Chem.* **1994**, *66*, 2809−2815.
(43) Mirgorodskaya, E.; O'Connor, P. B.; Costello, C. E. *J. Am. Soc. Mass Spectrom.* **2002**, *13*, 318−324.
(44) Domon, B.; Costello, C. E. *Glycoconjugate J.* **1988**, *5*, 397−409.

Table 1. Calculated *m/z* Values[a] for CS Precursor and Product Ions

	Δ-unsaturated	reduced Δ-unsaturated	saturated
precursor ion			
dimer $[M - H]^-$	458.061	461.083	476.071
tetramer $[M - H]^-$	917.129	920.151	935.140
tetramer $[M - 2H]^{2-}$	458.061	459.572	467.067
hexamer $[M - H]^-$	1376.198	1379.219	1394.208
hexamer $[M - 2H]^{2-}$	687.595	689.106	696.600
hexamer $[M - 3H]^{3-}$	458.061	459.068	464.064
product ion			
B_1^{1-}	157.014	157.014	175.024
B_2^{1-}	440.050	440.050	458.060
B_3^{1-}	616.082	616.082	634.092
B_4^{1-}	899.118	899.118	917.129
B_5^{2-}	537.071	537.071	546.076
C_1^{1-}	175.024	175.024	193.035
C_2^{1-}	458.060	458.060	476.071
C_3^{1-}	634.093	634.093	652.103
Y_1^{1-}	300.039	303.061	300.039
Y_2^{1-}	476.071	479.093	476.071
Y_3^{2-}	379.050	380.561	379.050
Y_4^{1-}	935.139	938.161	935.139
Z_1^{1-}	282.028	285.050	282.028
Z_2^{1-}	458.060	461.082	458.060
Z_4^{1-}	917.129	920.151	917.129

[a] All observed *m/z* values were within 8 ppm of calculated value.

gosaccharides at both the reducing and nonreducing termini. Therefore, the spectra of the reduced Δ-unsaturated derivatives were acquired to allow unambiguous assignment of ions based on observed *m/z*. The composition of Δ-unsaturated CS oligosaccharide will be given as Δ(*X*,*Y*,*Z*), where *X* = number of UroA residues, *Y* = number of GalNAc residues and *Z* = number of sulfate groups. The composition of reduced Δ-unsaturated CS oligosaccharides and the saturated CS oligosaccharides will be abbreviated Δ(*X*,*Y*,*Z*)OL and (*X*,*Y*,*Z*), respectively.

Nanospray FT-ICR Mass Spectra. The ESI-FT-ICR mass spectrum of each sample fraction was acquired. Representative mass spectra are displayed in Figure 1. In Figure 1A, the mass spectrum for the fraction containing the saturated tetramer from CSC depicts the presence of both the singly charged molecular ion, $[(2,2,2) - H]^{1-}$, at *m/z* 935.14 and the doubly charged molecular ion, $[(2,2,2) - 2H]^{2-}$ at *m/z* 467.07. Because sulfated oligosaccharides have a high affinity for alkali cations, ions corresponding to $[(2,2,2) + Na - 2H]^-$ and $[(2,2,2) + Na - 3H]^{2-}$ are observed in the mass spectrum, despite the fact that sodium was not added to the sample but was present in the sample at low concentrations. In addition, singly and doubly charged ions representative of (2,2,1) are observed. Ions having fewer sulfate groups than GalNAc residues are commonly observed in ESI mass spectra of CS oligosaccharides. Although these ions may arise via in-source fragmentation, sequences with fewer sulfates than GalNAc residues may also be present in solution. The singly charged molecular ion, $[\Delta(3,3,3) - H]^-$, at *m/z* 1376.20; the doubly charged molecular ion, $[\Delta(3,3,3) - 2H]^{2-}$, at *m/z* 687.60; and the triply charged molecular ion, $[\Delta(3,3,3) - 3H]^{3-}$, at *m/z* 458.06 for the Δ-unsaturated hexamer of CSC were observed in Figure 1B. As in Figure 1A, sodiated deprotonated hexamer ions are detected. Also present in this fraction are singly charged ions corresponding to the Δ-unsaturated tetramer.

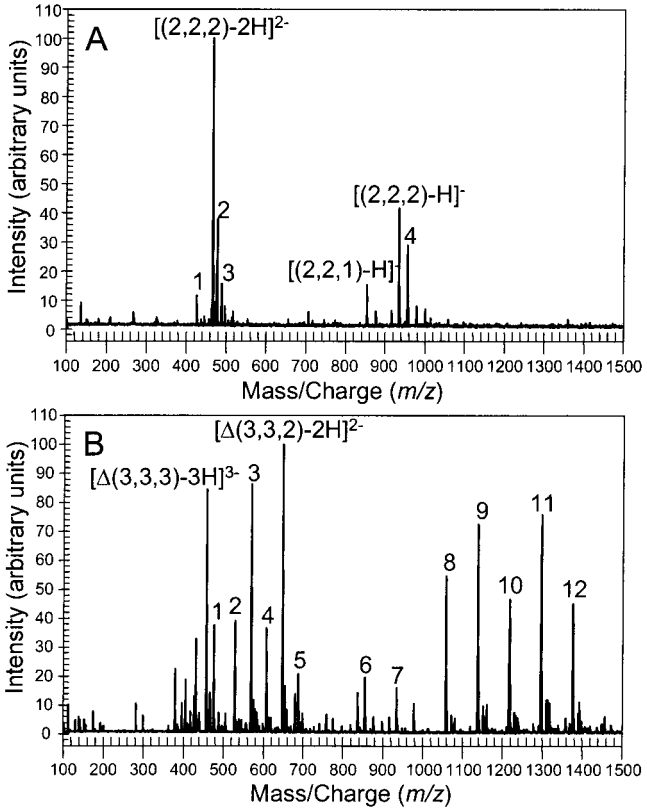

Figure 1. Negative ion ESI-FT-ICR mass spectra of a SEC fraction containing saturated CSC tetramer (A) and a SEC fraction containing Δ-unsaturated CSC hexamer (B). Additionally labeled ions in A are assigned as follows: 1, $[(2,2,1) - 2H]^{2-}$; 2, $[(2,2,2) + Na - 3H]^{2-}$; 3, $[(2,2,2) + 2Na - 4H]^{2-}$; and 4, $[(2,2,2) + Na - 2H]^-$. Additionally labeled ions in B are assigned as follows: 1, $[\Delta(3,3,3) + Na - 4H]^{3-}$; 2, $[\Delta(2,3,1) - 2H]^{2-}$ ($[Y_5 - 2SO_3]^{2-}$); 3, $[\Delta(2,3,2) - 2H]^{2-}$ ($[Y_5 - SO_3]^{2-}$); 4, $[\Delta(3,3,1) - 2H]^{2-}$; 5, $[\Delta(3,3,3) - 2H]^{2-}$; 6, $[(2,2,1) - H]^-$; 7, $[(2,2,2) - H]^-$; 8, $[\Delta(2,3,1) - H]^-$ ($[Y_5 - 2SO_3]^-$); 9, $[\Delta(2,3,2) - H]^-$ ($[Y_5 - SO_3]^-$); 10, $[\Delta(3,3,1) - H]^-$; 11, $[\Delta(3,3,2) - H]^-$; and 12, $[\Delta(3,3,3) - H]^-$. A peak corresponding to $[\Delta(2,3,3) - H]^-$ ($[Y_5]^-$) is present at *m/z* 1218.17 (not labeled).

It has been observed that the lability of sulfate groups in the gas phase follows the order $SO_3H > SO_3^- > SO_3Na$.[45] Although a deprotonated sulfate group is relatively stable and not likely to be lost from the precursor ion, a protonated sulfate group is easily lost from the precursor ion. In Figure 1B, the ESI-FT-ICR mass spectrum of a fraction containing Δ-unsaturated CSA hexamer demonstrates this phenomenon. The source conditions were energetic enough to produce ions corresponding to Y_5, $Y_5 - SO_3$, and $Y_5 - 2SO_3$ and those from losses of SO_3 from the precursor ion. The abundance of the $[\Delta(3,3,2) - 3H]^{3-}$ ion is less than that of the $[\Delta(3,3,3) - 3H]^{3-}$ ion. However, the abundance of the $[\Delta(3,3,2) - 2H]^{2-}$ ion is greater than the abundance of the $[\Delta(3,3,3) - 2H]^{2-}$ ion. Likewise, the observed abundances for the $[\Delta(3,3,2) - H]^-$ and $[\Delta(3,3,1) - H]^-$ ions are greater than that of the $[\Delta(3,3,3) - H]^-$ ion. These observations are consistent with loss of neutral SO_3 from doubly and singly charged ions produced from Δ(3,3,3).

ESI-FT-ICR SORI-CID Product Ion Mass Spectra of CS Disaccharides. It has been demonstrated that the sulfation

(45) Yagami, T.; Kitagawa, K.; Aida, C.; Fujiwara, H.; Futaki, S. *J. Pept. Res.* **2000**, *56*, 239−249.

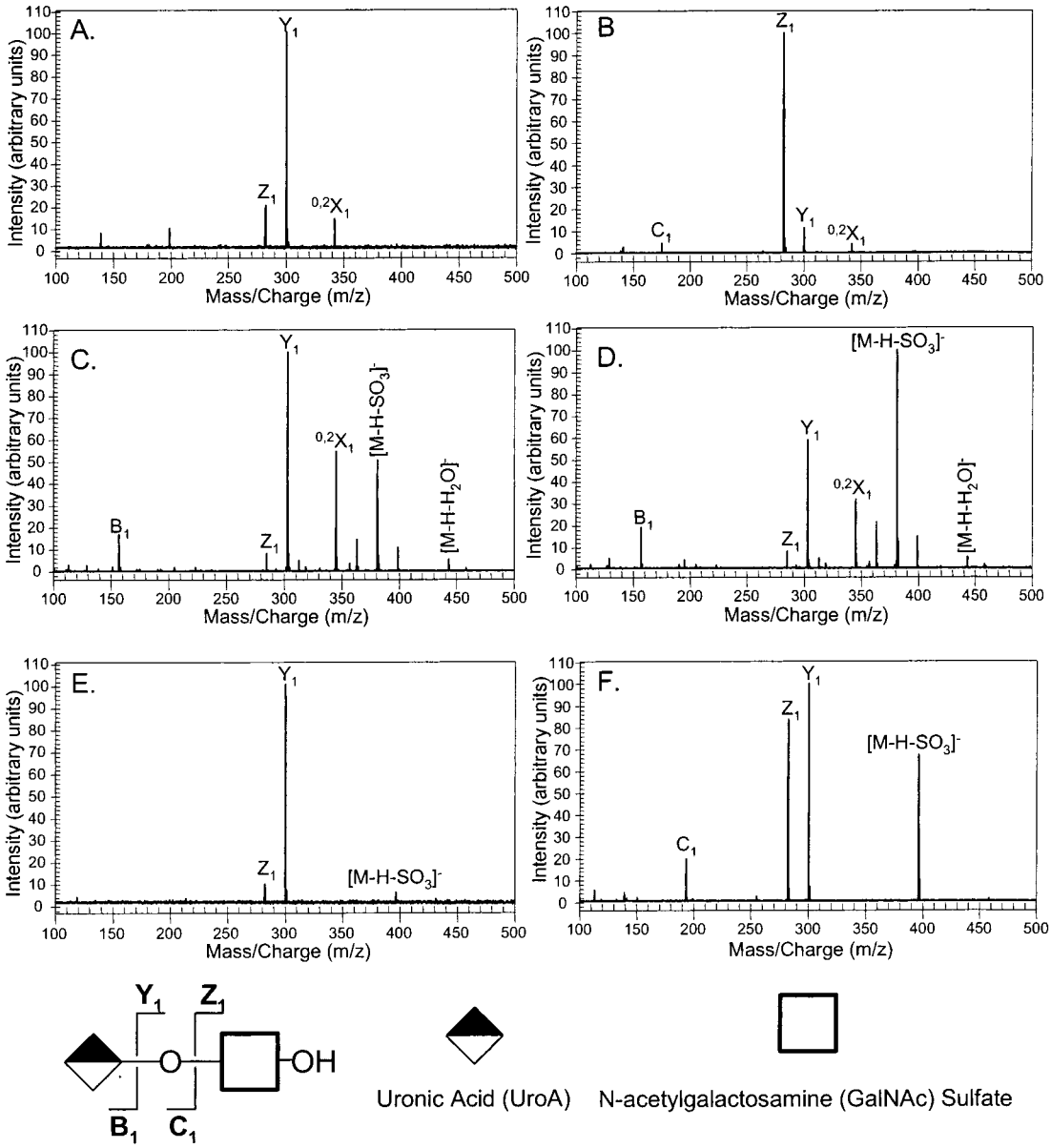

Figure 2. Negative ion ESI-FT-ICR SORI-CID product ion mass spectra of the (A) $[\Delta(1,1,1) - H]^-$ ion (*m*/*z* 458.06) of CSA, (B) $[\Delta(1,1,1) - H]^-$ ion (*m*/*z* 458.06) of CSC, (C) $[\Delta(1,1,1)OL - H]^-$ ion (*m*/*z* 461.08) of CSA, (D) $[\Delta(1,1,1)OL - H]^-$ ion (*m*/*z* 461.08) of CSC, (E) $[(1,1,1) - H]^-$ ion (*m*/*z* 476.07) of CSA, and (F) $[(1,1,1) - H]^-$ ion (*m*/*z* 476.07) of CSC. Excitation of each ion occurred at a frequency ~1.5% less than the ion of interest for a time period of 1000 ms and at an amplitude of 7 V. In the saturated CS disaccharide structure (below), the uronic acid (UroA) and *N*-acetylgalactosamine (GalNAc) sulfate are symbolized by the half-shaded diamond and the open square, respectively.

position, either 4S or 6S, can be determined for unsaturated CS disaccharides via ESI-MS/MS experiments on the quadrupole ion trap[36] and triple quadrupole[38] mass spectrometers. ΔDi4S ions dissociate to produce predominantly Y_1 ions at *m*/*z* 300.04 and $^{0,2}X_1$ ions, formed via cross-ring cleavage of the UroA at *m*/*z* 342.06. In contrast, ΔDi6S ions dissociate to produce predominantly z_1 ions at *m*/*z* 282.03.

In Figure 2, the SORI-CID product ion mass spectra for the singly charged ions produced by separate enzymatic digestion of CSA and CSC are displayed. The $[\Delta(1,1,1) - H]^-$ ions produced from the Δ-unsaturated disaccharides dissociate as expected. For the $[\Delta(1,1,1) - H]^-$ ion of CSA, which is primarily 4S, the Y_1 fragment ion is predominant in the product ion spectrum (Figure 2A). In contrast, the major fragment ion in the product ion spectrum of the $[\Delta(1,1,1) - H]^-$ ion of CSC, which is primarily 6S, is the Z_1 ion (Figure 2B). In the case of the ions corresponding to reduced Δ-unsaturated dimers from CSA and CSC, a different product ion pattern is observed for the $[\Delta(1,1,1)OL - H]^-$ ions. As evident in the product ion mass spectra for both the $[\Delta(1,1,1)$-$OL - H]^-$ ion of CSA (Figure 2C) and CSC (Figure 2D), both isomers dissociate to produce approximately the same Y_1:Z_1 fragment ion ratio. Furthermore, considerably more SO_3 loss and an increased relative abundance of the $^{0,2}X_1$ ion are observed for the flexible open-ring structures (Figure 2C,D) than for the constrained closed-ring structures (Figure 2A,B). The product ion mass spectrum of the saturated disaccharide ion $[(1,1,1) - H]^-$ (*m*/*z* 476.07) for CSA (Figure 2E) shows that the Z_1 ion is of low relative abundance, as is expected for the mostly 4-sulfated isomer. The Z_1 ion is observed at significantly greater relative abundance in the product ion mass spectrum of the saturated disaccharide

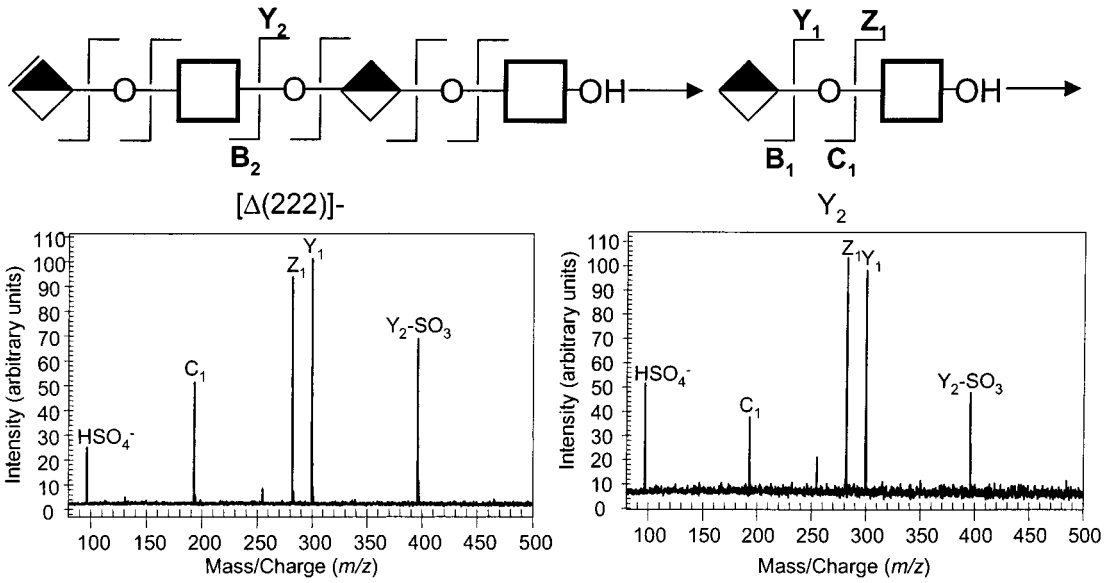

Figure 3. ESI-FT-ICR SORI-CID MS^3 product ion mass spectra of the Y_2 ion (*m*/*z* 476.07) from the $[(\Delta 2,2,2)]^-$ ion (*m*/*z* 917.13) from (A) CSA and (B) CSC. For each stage of MS, the excitation of each ion occurred at a frequency ~1.5% less than the ion of interest for a time period of 1000 ms and at an amplitude of 8 V.

ion for CSC (Figure 2F), but the Y_1:Z_1 ratio is not consistent with the trend exhibited by the dissociation of the disaccharide standards (Figure 2A,B).

Mechanistic studies have suggested that negative Y_n ions are formed with concomitant opening of the sugar ring to the nonreducing side.[44,46] It is therefore expected that changes to the structure of this ring will affect formation of Y_n ions. Evidently, the more constrained conformation of the Δ-unsaturated UroA residue of $\Delta[(1,1,1) - H]^-$ gives rise to Y_n ions, the abundances of which are sensitive to position of sulfation of the GalNAc residue. The less constrained saturated GlcA residue of $[(1,1,1) - H]^-$ allows for conformational flexibility that eliminates the sensitivity of Y_n ion abundances to sulfation position. The Y_2 ion (*m*/*z* 476.07) produced from tandem mass spectrometric dissociation of $[\Delta(2,2,2) - H]^-$ derived from CSA and CSC, respectively, was subjected to another stage of SORI-CID. The MS^3 product ion mass spectra (Figure 3) show the same pattern of product ions whether derived from CSA or CSC. The structure of the Y_2 ion does not appear to be the same as $[(1,1,1) - H]^-$, which is consistent with the conclusion that subsequent MS stages to fragment this ion are not likely to provide useful information regarding 4S/6S sulfation position.

ESI-FT-ICR SORI-CID Product Ion Mass Spectra of CS Tetrasaccharides. In Figure 4, the ESI-FT-ICR SORI-CID product ion spectra for the doubly charged ions produced from the purified CS tetrasaccharides are shown. The product ion mass spectrum of the $[\Delta(2,2,2) - 2H]^{2-}$ ion of CSA (Figure 4A) shows abundant ions corresponding to cleavage at the bond that yields B_3 and Y_1. By comparison, the product ion mass spectrum of the $[\Delta(2,2,2) - 2H]^{2-}$ ion from CSC (Figure 4B) shows abundant ions corresponding to Z_1, B_3, Y_1, and C_3. Both spectra are consistent with the most probable bond cleavage occurring at the reducing terminal glycosidic bond observed for fully charged CS oligosaccharides.[39] The identity of the product ions is confirmed by comparison with the product ion spectra of the $[(\Delta 2,2,2)OL - 2H]^{2-}$ ion (Figure 4C) and $[(2,2,2) - 2H]^{2-}$ ion (Figure 4D) from CSA. The *m*/*z* values of Y_n and Z_n ions are shifted in the product ion spectrum for the reduced Δ-unsaturated molecule versus the Δ-unsaturated and saturated molecules. (See Table 1.) The *m*/*z* values of B_n and C_n ions are shifted in the product ion spectrum of the saturated molecule as compared to the Δ-unsaturated and reduced Δ-unsaturated molecules. These *m*/*z* shifts allow for the confirmation of the product ions' identity. The increased ion abundance of the Y_3^{2-} ion in Figure 4D, relative to Figure 4A, is consistent with the supposition that its abundance is influenced by the structure of the UroA residue to the nonreducing side.

Product ion mass spectra of singly charged ions produced from tetramers of enzymatically digested CSA and CSC are presented in Figure 5. The product ion mass spectrum of the $[\Delta(2,2,2) - H]^-$ ion of CSA (Figure 5A) shows abundant ions corresponding to $[\Delta(2,2,2) - H - SO_3]^-$, Y_2, and B_2. By comparison, the product ion mass spectrum of the $[\Delta(2,2,2) - H]^-$ ion of CSC (Figure 5B) shows abundant ions corresponding to $[\Delta(2,2,2) - H - SO_3]^-$ and Y_2. Low abundance ions in this spectrum include those corresponding to B_2 and sulfate-adducted Y_2 and B_2. The identity of the Y_2 ion was confirmed from the product ion mass spectra for the $[\Delta(2,2,2)OL - H]^-$ from CSA (Figure 5C) and CSC (Figure 5D), for which the *m*/*z* value is shifted by the reducing step. The identity of the B_2 ion was confirmed from the product ion mass spectra for the $[(2,2,2) - H]^-$ ion of CSA (Figure 5E) and CSC (Figure 5F), in which the nonreducing terminus is saturated and results in a *m*/*z* shift for the B_2 ion relative to the Δ-unsaturated molecule. Interestingly, there is a significant difference in the B_2:Y_2 ion ratio produced by the dissociation of the $[\Delta(2,2,2) - H]^-$ ion from CSA versus CSC (Table 2). This observation is consistent with the conclusion that the position of the sulfate, either 4S or 6S, on the GalNAc at position 3 mediates the dissociation pathway.

(46) Prome, J. C.; Aurelle, H.; Prome, D.; Savagnac, A. *Org. Mass Spectrom.* **1987**, *22*, 6−12.

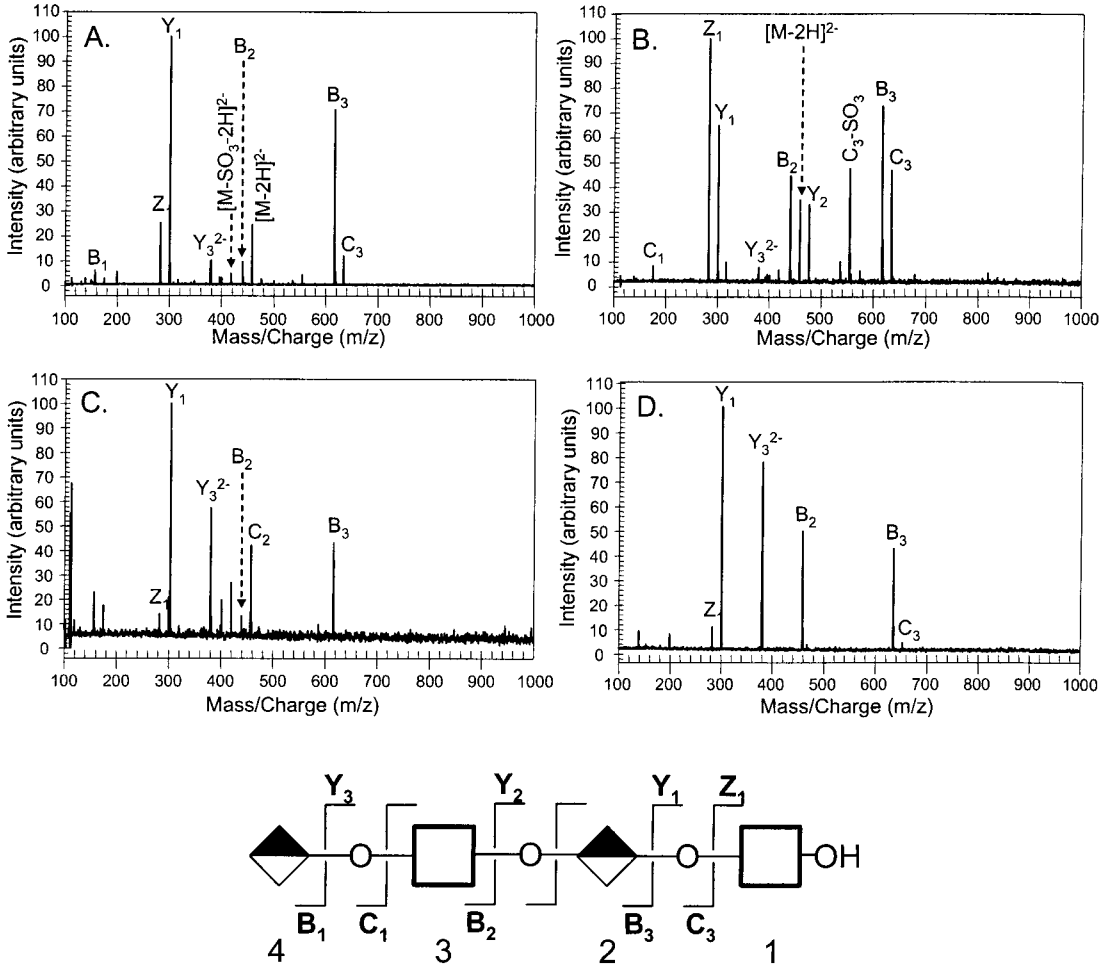

Figure 4. Negative ion ESI-FT-ICR product ion mass spectra of the (A) $[\Delta(2,2,2) - 2H]^{2-}$ ion (*m*/*z* 458.06) of CSA, (B) $[\Delta(2,2,2) - 2H]^{2-}$ ion (*m*/*z* 458.06) of CSC, (C) $[\Delta(2,2,2)OL - 2H]^{2-}$ ion (*m*/*z* 459.07) of CSA, and (D) $[(2,2,2) - 2H]^{2-}$ ion (*m*/*z* 464.06) of CSA. Excitation of each ion occurred at a frequency ~1.5% less than the ion of interest for a time period of 1000 ms and at an amplitude of 7 V.

Table 2. Comparison of Glycosidic Bond Cleavages for Singly Charged Ions Produced from CSA and CSC Digests

	product ion ratio			
precursor ion	Z_1^-:Y_1^-	ΣB_2^-:ΣY_2^- [a]	ΣB_4^-:ΣY_2^- [a]	ΣB_4^-:ΣY_4^- [a]
CSA $[\Delta(111) - H]^-$	0.21			
CSC $[\Delta(111) - H]^-$	9.10			
CSA $[\Delta(222) - H]^-$		0.61		
CSC $[\Delta(222) - H]^-$		0.18		
CSA $[\Delta(333) - H]^-$			5.01	2.08
CSC $[\Delta(333) - H]^-$			2.66	4.90
CSA $[\Delta(333) - 2H]^{2-}$			0.56	0.80
CSC $[\Delta(333) - 2H]^{2-}$			0.80	$B_4 \gg$

[a] The sum (Σ) of selected ions includes all associated ions occurring from the specific glycosidic bond cleavage, including $[P + SO_3]$ and $[P - SO_3]$.

The product ion patterns for the singly charged ions differ dramatically from those of the corresponding doubly charged ions presented in Figure 4A,B. Differences include a much greater abundance of ions produced from loss of SO_3 or H_2SO_4 loss from the precursor ion, formation of B_2 and Y_2 ions rather than odd-numbered B_n and Y_n ions, and the generation of product ions containing an additionally adducted sulfate group. The B_2 and Y_2 ions are formed from glycosidic bond cleavages to the reducing side of the GalNAc residue in position 3, and their *m*/*z* values are consistent with sulfated structures. Thus, for the population of precursor ions with a deprotonated sulfate on the GalNAc residue at position 3, glycosidic bond cleavage results in a B_2 ion. For ions with a deprotonated sulfate on the reducing terminal GalNAc residue, glycosidic bond cleavage results in the formation of a Y_2 ion. The protonated sulfate group is rather labile, as shown by the high abundance of ions formed by the loss of SO_3 and H_2SO_4 from the precursor ion.

These observed differences in product ion spectra are consistent with the conclusion that the singly and doubly charged ions have significantly different conformations, producing different fragmentation patterns. The doubly charged ion would be expected to adopt an extended conformation to keep the charge separated. More compact conformations would be possible for the singly charged ions. The data are consistent with transfer of a protonated sulfate group to an oxygen atom elsewhere in the molecule prior to (or concurrent with) glycosidic bond cleavage. For ions with charge residing on the GalNAc at position 2, the neutral SO_3 is transferred from the GalNAc at position 1 and glycosidic bond cleavage forms $[B_2 + SO_3]^-$, an ion that readily loses a SO_3 group to form the B_2 ion. For ions with charge state

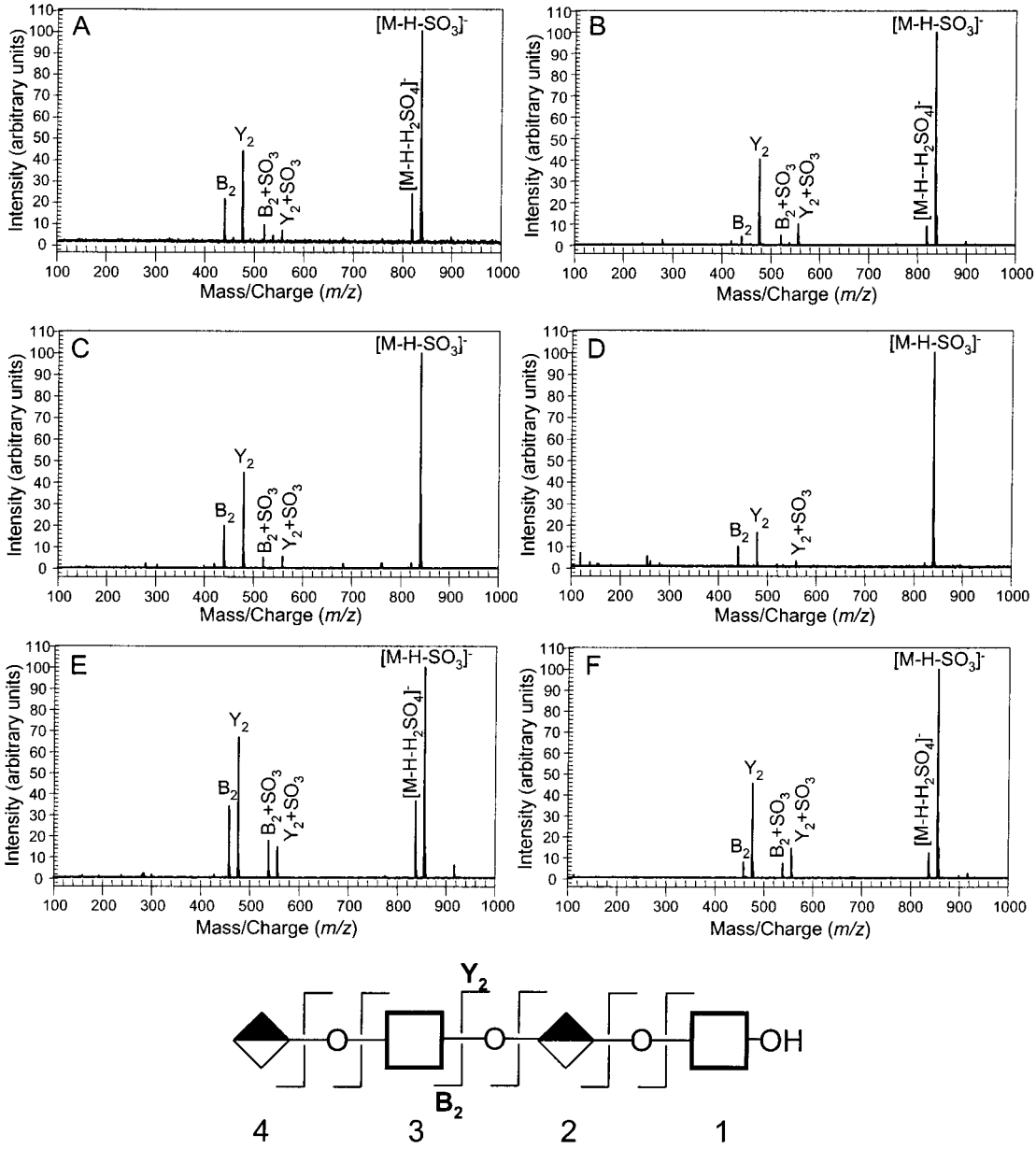

Figure 5. Negative ion ESI-FT-ICR SORI-CID product ion mass spectra of the (A) $[\Delta(2,2,2) - H]^-$ ion (*m*/*z* 917.13) of CSA (B), $[\Delta(2,2,2) - H]^-$ ion (*m*/*z* 917.13) of CSC, (C) $[\Delta(2,2,2)OL - H]^-$ ion (*m*/*z* 920.15) of CSA, (D) $[\Delta(2,2,2)OL - H]^-$ ion (*m*/*z* 920.15) of CSC, (E) $[(2,2,2) - H]^-$ ion (*m*/*z* 935.14) of CSA, and (F) $[(2,2,2) - H]^-$ ion (*m*/*z* 935.14) of CSC. Excitation of each ion occurred at a frequency ~1.5% lower than the ion of interest for a time period of 1000 ms and at an amplitude of 8 V.

residing on the GalNAc residue at position 1, SO_3 is transferred from GalNAc at position 3, and glycosidic bond cleavage forms the $[Y_2 + SO_3]^-$ ion, and subsequent loss of SO_3 produces Y_2.

ESI-FT-ICR SORI-CID Product Ion Mass Spectra of CS Hexasaccharides. The ESI-FT-ICR SORI-CID product ion mass spectra for singly charged ions produced from the purified CS hexasaccharides are displayed in Figure 6. The product ion mass spectrum of the $[\Delta(3,3,3) - H]^-$ ion of CSA (Figure 6A) shows abundant ions corresponding to $[\Delta(3,3,3) - H - SO_3]^-$, $[\Delta(3,3,3) - H - H_2SO_4]^-$, $[\Delta(3,3,3) - H - H_2O]^-$, Z_4, B_4, and Y_4. Similarly, the product ion mass spectrum of the $[\Delta(3,3,3) - H]^-$ ion of CSC (Figure 6B) shows abundant ions corresponding to $[\Delta(3,3,3) - H - SO_3]^-$, $[\Delta(3,3,3) - H - H_2SO_4]^-$, $[\Delta(3,3,3) - H - H_2O]^-$, B_4, Z_4, and Y_4. Low abundance ions in these spectra include those corresponding to Y_2 and sulfate adducted to B_4 and Z_4. The identity of the Y_n and Z_n ions were confirmed by comparison of the product ion spectra of the $[\Delta(3,3,3) - H]^-$ ions with the product ion spectra of the $[\Delta(3,3,3)OL - H]^-$ ions from CSA (Figure 6C) and CSC (Figure 6D). The identity of the B_n ions was confirmed by comparison of the product ion spectra of the $[\Delta(3,3,3) - H]^-$ ions with the product ion spectra of the $[(3,3,3) - H]^-$ ions from CSA (Figure 6E) and CSC (Figure 5F). Via comparison of the product ion spectra for the $[\Delta(3,3,3)OL - H]^-$ ions and $[(3,3,3) - H]^-$ ions, it was determined that there are no C_n ions present in the spectra. Comparison of the ratios for the B_n and Y_n ions in the product ion spectra of CSA and CSC indicates that the sulfate position impacts the dissociation of the ion and the production of these fragment ions (Table 2).

In Figure 6, the most abundant glycosidic bond cleavage product ions are B_4, Z_4, Y_4, and Y_2. The Z_4 and Y_4 ions result from

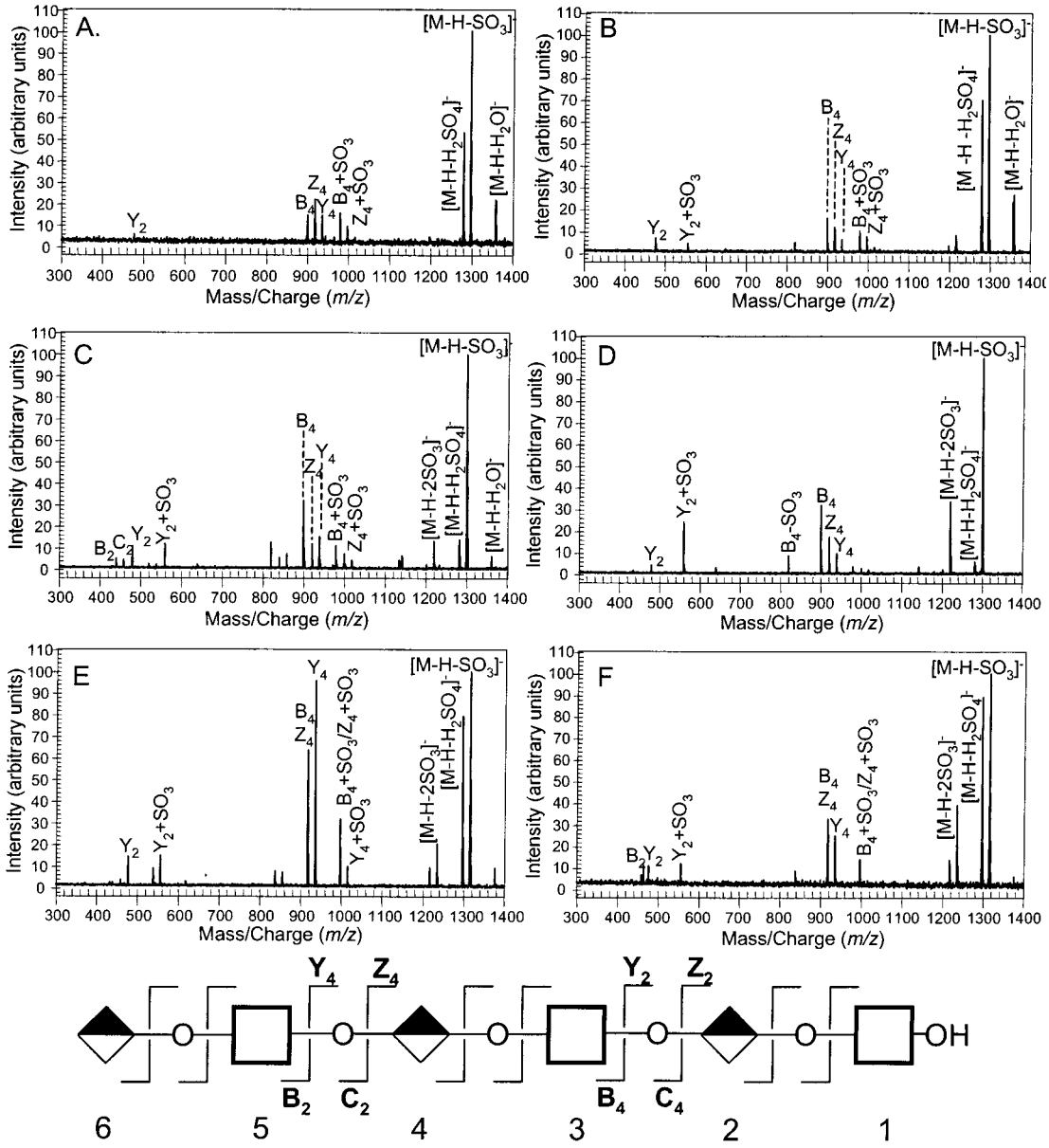

Figure 6. Negative ion ESI-FT-ICR SORI-CID product ion mass spectra of the (A) $[\Delta(3,3,3) - H]^-$ ion (*m*/*z* 1376.20) of CSA, (B) $[\Delta(3,3,3) - H]^-$ ion (*m*/*z* 1376.20) of CSC, (C) $[\Delta(3,3,3)OL - H]^-$ ion (*m*/*z* 1379.22) of CSA, (D) $[\Delta(3,3,3)OL - H]^-$ ion (*m*/*z* 1379.22) of CSC, (E) $[(3,3,3) - H]^-$ ion (*m*/*z* 1394.21) of CSA, and (F) $[(3,3,3) - H]^-$ ion (*m*/*z* 1394.21) of CSC. Excitation of each ion occurred at a frequency ~1.5% lower than the ion of interest for a time period of 1000 ms and at an amplitude of 6 V.

cleavage to the reducing side of the GalNAc in position 5. The B_4 and Y_2 ions result from cleavage to the reducing side of the GalNAc in position 3. The ion corresponding to B_2 is at low relative abundance, consistent with the conclusion that very few of the precursor ions are present with charge residing on the GalNAc at position 5. The low abundance of the Y_2 ion is consistent with the conclusion that few precursor ions exist with charge residing at the GalNAc at position 1. This pattern is consistent with the conclusion that charge resides primarily on the GalNAc at position 3. Intramolecular transfer of neutral SO_3 is observed for ions corresponding to $B_4 + SO_3$, $Y_4 + SO_3$, $Z_4 + SO_3$, and $Y_2 + SO_3$.

In Figure 7, the SORI-CID product ion mass spectra of doubly and triply charged CS hexasaccharide ions are compared. The product ion mass spectrum of the $[\Delta(3,3,3) - 3H]^{3-}$ ion of CSA (Figure 7A) shows abundant ions corresponding to $[\Delta(3,3,3) - 2H - SO_3]^{2-}$, B_2, Y_4, B_4, Y_2, Z_1, and Y_1. Similarly, the product ion mass spectrum of the $[\Delta(3,3,3) - 2H]^{2-}$ ion of CSC (Figure 7B) shows abundant ions corresponding to Y_2, $[\Delta(3,3,3) - 2H - SO_3]^{2-}$, B_4, B_2, and Z_1. The presence of the abundant Y_2 ion indicates that a large fraction of ions are produced with charge localized on the sulfate groups on the GalNAc at position 1, and the abundant B_2 ion is consistent with charge localization on the GalNAc at position 5. The localization of charge on GalNAc residue at positions 1 and 5 allows for separation of charge. Loss of SO_3 observed from B_4 and Y_4 is expected, since only one of the sulfate groups in these ions is charged. Significantly, intramolecular transfer of SO_3 is not observed. This observation is consistent with the conclusion that an extended conformation minimizes the extent of SO_3 transfer prior to or concurrent with glycosidic bond cleavage.

Odd-numbered B_n and Y_n ions are observed in product ion mass spectra of $[\Delta(3,3,3) - 3H]^{3-}$, which is consistent with

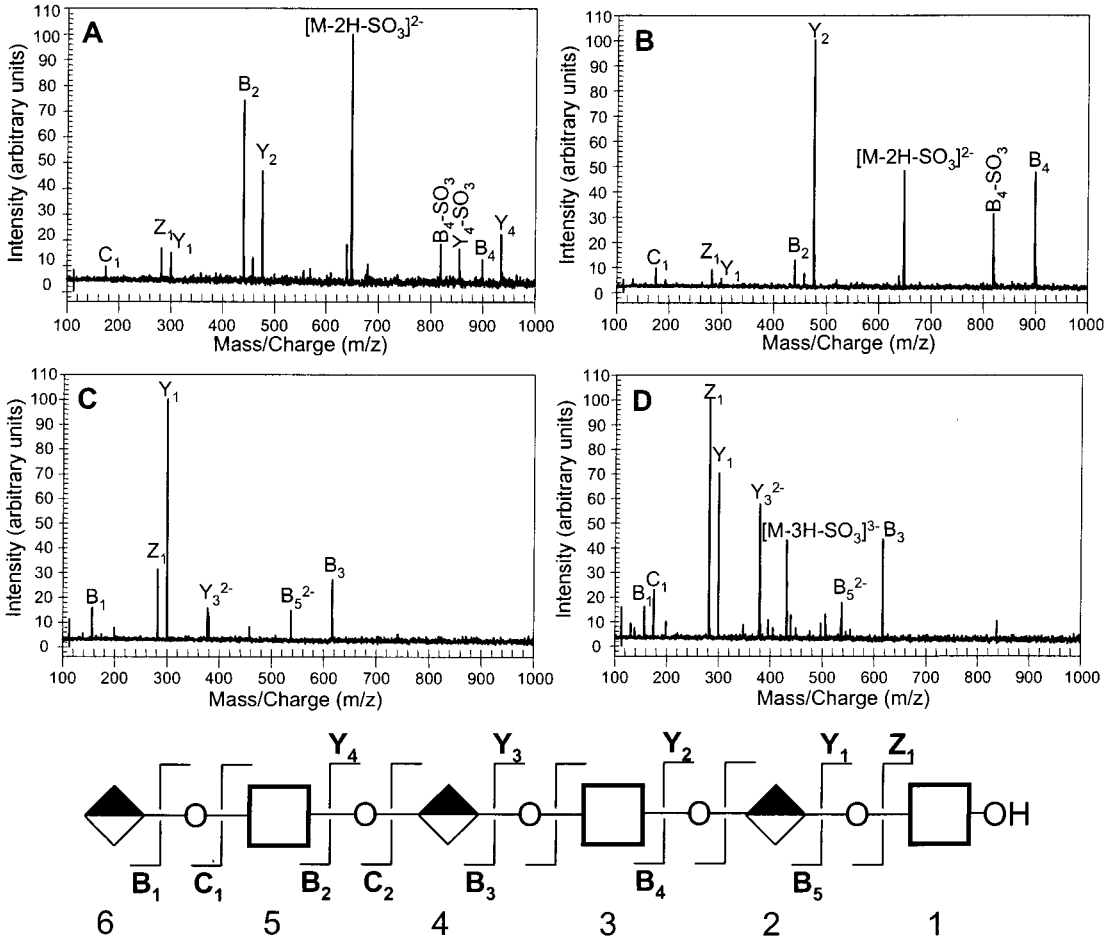

Figure 7. Negative ion ESI-FT-ICR SORI-CID product ion mass spectra of the (A) $[\Delta(3,3,3) - 2H]^{2-}$ ion (*m*/*z* 687.60) of CSA, (B) $[\Delta(3,3,3) - 2H]^{2-}$ ion (*m*/*z* 687.60) of CSC, (C) $[\Delta(3,3,3) - 3H]^{3-}$ ion (*m*/*z* 458.06) of CSA, (D) $[\Delta(3,3,3) - 3H]^{3-}$ ion (*m*/*z* 458.06) of CSC. Excitation of each ion occurred at a frequency ~1.5% lower than the ion of interest for a time period of 1000 ms and at amplitudes of 7 V and 6 V for the doubly charged and triply charged ions, respectively.

previous observations.[39] The product ion mass spectrum of the $[\Delta(3,3,3) - 3H]^{3-}$ ion of CSA (Figure 7C) shows abundant ions corresponding to Y_1, Z_1, B_3, B_5^{2-}, Y_3^{2-}, and B_1. Similarly, the product ion mass spectrum of the $[\Delta(3,3,3) - 2H]^{2-}$ ion of CSC (Figure 7D) shows abundant ions corresponding to Z_1, Y_1, Y_3^{2-}, B_3, B_5^{2-}, C_1, and B_1. Ions corresponding to loss or intramolecular transfer of SO_3 are not observed. Although both the triply and doubly charged ions are likely to adopt extended conformation in the gas phase, the observed patterns of glycosidic bond cleavages are dramatically different. The presence of three charged GalNAc residues results in the formation of odd-numbered B_n and Y_n ions (Figure 7C and 6D). The presence of an uncharged GalNAc residue at position 3 for the doubly charged ions results in even-numbered B_n and Y_n ions (Figures 7A and 6B). Given that GalNAc residues 1 and 5 are charged in both cases, it seems unlikely that the presence of charge on a given sulfate determines whether glycosidic bond cleavage occurs to the nonreducing or the reducing side of the GalNAc. It therefore seems likely that the location of charge relative to cleaved glycosidic bonds does not determine whether odd-numbered or even-numbered B_n and Y_n ions are observed. Odd-numbered ions are observed only when all sulfate groups are charged. These observations are consistent with the conclusion that the $[\Delta(3,3,3) - 3H]^{3-}$ ion adopts a unique conformation necessary to maximize charge separation that disfavors formation of even-numbered B_n and Y_n ions.

Comparison of Precursor Ion Dissociation Methods. In Figure 8, the fragmentation patterns of the $[\Delta(3,3,3) - H]^-$ ion from CSC upon dissociation by either SORI-CID or IRMPD are compared. The product ion mass spectrum acquired using SORI-CID (Figure 8A) shows abundant ions corresponding to $[\Delta(3,3,3) - H - SO_3]^-$, $[\Delta(3,3,3) - H - H_2SO_4]^-$, $[\Delta(3,3,3) - H - H_2O]^-$, B_4, Z_4, Y_4, and Y_2. The product ion mass spectrum acquired using IRMPD (Figure 8B) shows abundant ions corresponding to $[\Delta(3,3,3) - H - SO_3]^-$, $[\Delta(3,3,3) - H - H_2SO_4]^-$, $[\Delta(3,3,3) - H - 2SO_3]^-$, $[\Delta(3,3,3) - H - 2H_2SO_4]^-$, $[\Delta(3,3,3) - H - H_2O]^-$, Z_2^{int}, Y_2, Y_4, Z_4, B_4, and B_2. In the SORI-CID product ion mass spectrum, the precursor ion is completely dissociated, whereas in the IRMPD spectrum, the precursor ion is still present. The dissociation of the precursor ion via IRMPD resulted in the formation of secondary fragment ions, B_2 and an internal fragment ion, Z_2^{int} (*m*/*z* 458.06), the increased relative abundance of the Y_2 ion, and multiple losses of SO_3 and H_2SO_4 from the precursor ion. Of particular concern is the formation of the Z_2^{int} ion as the result of multiple fragmentations, which has been shown to be an indicator ion for over-fragmentation in previous studies.[39] The observance of these ions indicates that the trapped ions in the ICR cell are undergoing multiple fragmentations. The observation of abundant

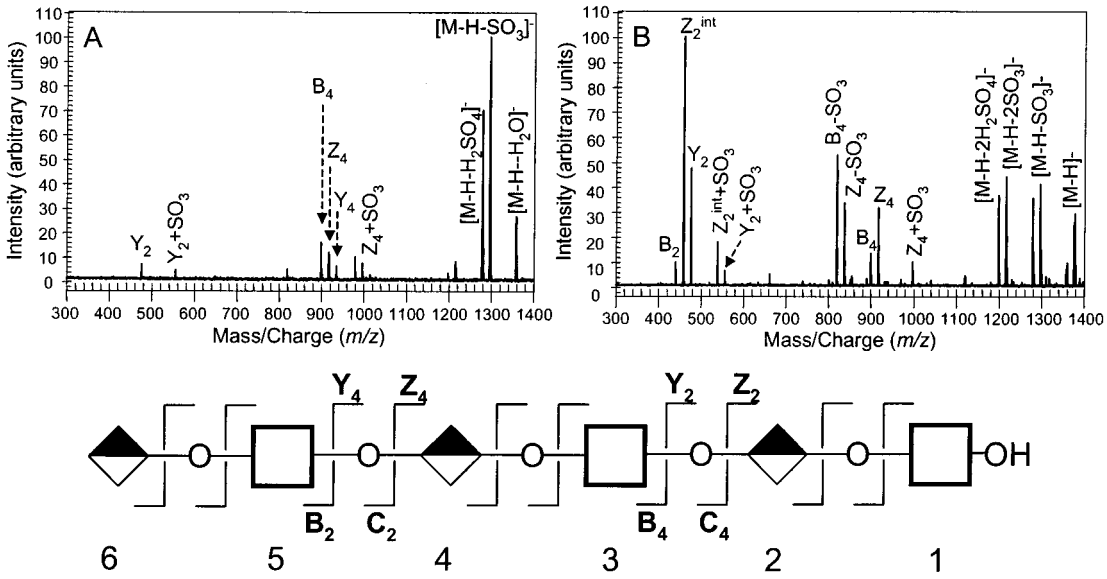

Figure 8. Comparison of negative ion ESI-FT-ICR product ion spectra of $[\Delta(3,3,3) - H]^-$ ion from CSC produced by (A) SORI-CID and (B) IRMPD. The conditions for dissociation by SORI-CID were an excitation time of 1000 ms and an excitation amplitude of 6 V. The dissociation by IRMPD used a laser power of 100% applied for 450 ms.

internal fragment ions is consistent with the conclusion that IRMPD is disadvantageous relative to SORI-CID as a means of fragmenting CS oligosaccharides. As results in this paper have demonstrated, the selective nature of SORI-CID fragmentation results in internal fragment ions that are of very low abundance.

CONCLUSION

The observed product ion patterns in MS/MS spectra of CS oligosaccharides vary dramatically with ion charge state. The product ion spectra of singly charged CS ions (Figures 5 and 6) are characterized by even-numbered B_n and Y_n ions and intramolecular transfer of neutral SO_3. Apparently, this transfer occurs for such ions because the conformation is compact and conducive to the migration of the SO_3 to an oxygen atom of a different residue. The spectra of doubly charged CS hexamers (Figure 7A, B) indicate that the juxtaposed charges on GalNAc sulfate residues at positions 1 and 5 result in more extended conformations that prevent intramolecular contacts necessary for sulfate transfer.

The B_2 and Y_4 ions observed in Figure 7A,B result from glycosidic bond cleavage to the reducing side of the charged GalNAc sulfate residue at position 5. By contrast, the Y_2 and B_4 ions result from cleavage to the reducing side of an uncharged GalNAc sulfate residue. This observation implies that the presence of charge on a GalNAc sulfate residue does not directly determine whether glycosidic cleavage occurs on the reducing side. Product ion mass spectra of CS oligosaccharides for which z is the number of sulfate groups (Figures 4A,B, 7C,D) produce predominantly odd-numbered B_n and Y_n ions resulting from glycosidic bond cleavage to the reducing side of the GlcA residues. This pattern appears to result from the conformation of the fully charged ions, as distinct from that of ions for which $z <$ the number of sulfates. Such a conformational difference would explain the dramatically higher abundances in the Y_1^- ions in spectra of $[\Delta(3,3,3) - 3H]^{3-}$ (Figure 6A,B) versus $[\Delta(3,3,3) - 2H]^{2-}$ (Figure 7A,B) ions when both ions have charge localized to the GalNAc sulfate at position 1.

These studies have important implications for the analysis of the pattern of sulfation in oligosaccharides derived from CS. For ions where z is the number of sulfate groups, it has not been possible to determine the position of sulfation of the GalNAc residue adjacent to the nonreducing terminal GlcA residue.[39] The observation of abundant B_2 and Y_2 ions in the spectra of $[\Delta(2,2,2) - H]^-$, however, shows that product ions resulting from glycosidic bond cleavage to the reducing side of this residue are formed. The abundances of these ions reflect the positions of sulfation, as shown in Table 2. Thus, complete analysis of the sulfation positions of CS tetramers and hexamers can be accomplished by acquiring tandem mass spectra of the 3^- and 2^- charge states. Comparison of B_n and Y_n ion abundances with those generated from standard preparation of oligosaccharides from CSA and CSC will allow assignment of positions of sulfation. A similar scheme is expected to be useful for the analysis of larger CS oligosaccharides. For these ions, it is not yet clear which will be the optimal charge state for generation of even-numbered B_n and Y_n ions without observing intramolecular sulfate transfer. Studies to resolve these questions are in progress.

For ions generated from GAG oligosaccharides in which protonated sulfate groups are present (total charge $z <$ the number of sulfate groups), intramolecular sulfate migration is possible. These studies demonstrate that migration does not occur in CS hexamers when there are at least two charged sulfate groups on the ion, causing the ions to adopt an extended gas-phase conformation. Additional studies are required to determine whether intramolecular sulfate migration will be observed for longer CS oligosaccharide ions in which there are two charges or whether a higher charge state will be necessary to avoid this phenomenon. Because they contain a greater number of sulfate groups per disaccharide residue relative to CS oligosaccharides the most abundant charge states generated from heparin oligosaccharides are likely to have a total charge that is less than the number of sulfate groups. The results of these studies are

consistent with the conclusion that intramolecular sulfate migration can be minimized in the analysis of heparin oligosaccharides by using electrospray solution and source conditions that minimize the number of protonated sulfate groups. This can be accomplished by using a low percent of ammonium hydroxide in the ionization solution and by carefully positioning the nanospray needle. Tandem mass spectrometric studies are in progress to elucidate the product ion patterns of heparin oligosaccharides.

Abbreviations Used. CID, collision-induced dissociation; CS, chondroitin sulfate; CSA, chondroitin sulfate type A; CSC, chondroitin sulfate type C; ΔDi4S, ΔUroA(β1,3)-D-GalNAc4S; ΔDi6S, ΔUroA(β1,3)-D-GalNAc6S; ESI, electrospray ionization; FAB, fast atom bombardment; FT-ICR, Fourier transform-ion cyclotron resonance; GAG, glycosaminoglycan; GalNAc, *N*-acetylgalactosamine; GlcA, glucuronic acid; HPLC, high-performance liquid chromatography; IdoA, iduronic acid; IRMPD, infrared multiphoton dissociation; MALDI, matrix-assisted laser desorption/ionization; MS, mass spectrometry; MS/MS, tandem mass spectrometry; NMR, nuclear magnetic resonance; SEC, size exclusion chromatography; SORI-CID, sustained off-resonance irradiation collision-induced dissociation; TOF, time-of-flight; UroA, uronic acid

ACKNOWLEDGMENT

This work was supported by NIH/NCRR Grant No. P41-RR10888.

Received for review January 7, 2002. Accepted May 14, 2002.

AC025506+